Synthesis of *N*-phenethyl-*p*-methoxycinnamamide and *N*-morpholinyl-*p*-methoxycinnamamide, *In Vitro* and *In Silico* Study as α-Glucosidase Inhibitor

Herlina Rasyid[1*], Firdaus Firdaus[1], Syadza Firdausiah[1], Nunuk Hariani Soekamto[1], Seniwati Seniwati[1], Riska Mardiyanti[1], Reynaldi Reynaldi[1], Andi Eka Sri Rahayu[1], and Wahyu Dita Saputri[2]

[1]*Department of Chemistry, Faculty of Mathematics and Natural Sciences, Hasanuddin University, Jl. Perintis Kemerdekaan km 10, Makassar 90245, South Sulawesi, Indonesia*

[2]*Research Center for Quantum Physics, National Research and Innovation Agency (BRIN), Habibie Science and Technology Complex (Puspiptek), Serpong 15314, South Tangerang, Indonesia*

* ***Corresponding author:***

tel: +62-85255606583
email: herlinarasyid@unhas.ac.id

Received: August 2, 2022
Accepted: October 5, 2022

DOI: 10.22146/ijc.76802

Abstract: *Aromatic ginger (*Kaempferia galanga *L.) is one of the natural sources containing ethyl-*p*-methoxycinnamate, which is known to have beneficial activity, especially as an α-glucosidase inhibitor. This study aims to convert ethyl-*p*-methoxycinnamate into amide form as* N*-phenethyl-*p*-methoxycinnamamide (**4a**) and* N*-morpholinyl-*p*-methoxycinnamamide (**4b**) through some synthetic ways then tested their activity as an α-glucosidase inhibitor. The FTIR spectra of **4a** present a short single peak at 3269.34 cm^{-1} that belongs to the N-H group, while spectra of **4b** show no absorption band between 3200–3400 cm^{-1} due to its tertiary amide structure. Spectroscopy analysis through ^{1}H- and ^{13}C-NMR exhibits the successful synthesis of both compounds. Bioactivity test results show that compound **4b** has better activity than **4a**. In molecular dynamics simulation, the binding energy of compounds **4a** and **4b** reveal that both compounds have a similar binding energy of about -98980.8 and -97696.7 kJ mol^{-1}, respectively.*

Keywords: *aromatic ginger (*Kaempferia galanga *L.); cinnamamide derivatives; α-glucosidase inhibitor; molecular docking; MD simulation*

■ INTRODUCTION

Aromatic ginger (*Kaempferia galanga* L.) is one of the traditional medicine which is known to contain ethyl-*p*-methoxycinnamate (EPMC) [1], ethyl cinnamate [2], isopimarane-type diterpenoids [3-4]. The other chemical compounds were δ-3-carene, 1,8-cineole, borneol, and pentadecane [5]. The two most abundant compounds in the aromatic ginger essential oil were trans-ethyl-*p*-methoxycinnamate and trans-ethyl cinnamate [1-2,5]. Ethyl-*p*-methoxycinnamate and its derivatives had many benefits, including as anticancer [6-8], anti-inflammatory [9-10], anti-tuberculosis [11], anti-neoplastic [12], antimicrobe [13], and antidiabetic [14] agents. The study of *K. galanga* L. extract as an antidiabetic using the Gavage method every day for one month found that diabetic rats before and after treatment with *K. galanga* L. extract showed a significant difference in reducing the amount of blood glucose [15].

In addition, the cinnamic acid derivative compound had an antidiabetic activity which had been shown to reduce plasma glucose concentrations in diabetic rats by reducing the excessive activity of glucose-6-phosphatase, hepatic hexokinase, glucokinase, and phosphofructokinase and increasing liver glycogen in diabetic rats but did not change plasma glucose concentrations in normal rats. The antihyperglycemic effect of *p*-methoxy cinnamic acid worked by increasing insulin secretion and glycolysis and reducing gluconeogenesis [16] and significantly inhibited the formation of advanced glycation end products (AGEs). This result proved that cinnamic acid and its derivatives could effectively protect BSA from

fructose by mediated protein glycation and reduced fructosamine level [17].

Other studies showed that the conversion of cinnamic acid to amide form gave a better activity as an antidiabetic, especially inhibition of α-glucosidase [18-20]. This research started with the isolation of ethyl-*p*-methoxycinnamate from aromatic ginger and, through some synthetic ways, changed to amide form by using phenethylamine and morpholine. The synthesized compounds were continued to *in vitro* analysis as an α-glucosidase inhibitor and *in silico* analysis by using homology modeling [21], molecular docking [22-24], and stability analysis through molecular dynamics simulation [25-26].

■ EXPERIMENTAL SECTION

Materials

Materials used in this research were *p*-methoxycinnamic acid, benzene, thionyl chloride, pyridine, triethylamine (TEA), phenethylamine, morpholine, HCl 3%, NH_4Cl, chloroform, ethyl acetate, *n*-hexane, anhydrous Na_2SO_4, *p*-nitrophenyl-α-D-glucopyranoside, α-glucosidase enzyme, Na_2CO_3, and buffer phosphate pH 7.

Instrumentation

Instrumentations utilized were Fourier-Transform Infrared (FTIR) and Nuclear Magnetic Resonance (NMR) spectroscopy. The FTIR spectra were recorded using Spectrophotometer Shimadzu Prestige 21, while the ^{1}H-NMR spectra were obtained by using Spectrometer Agilent operating at 500 MHz and 125 MHz for ^{1}H- and ^{13}C-NMR, respectively. The melting points of each crystal were counted on the electrothermal apparatus.

Procedure

Conversion method

In this stage, there were two cinnamamide derivatives converted. The conversion method scheme is shown in Fig. 1. The procedure was started by isolating ethyl-*p*-methoxycinnamate (**1**) from aromatic ginger (*Kaempferia galanga* L.). Then it was converted into the amide derivatives by some synthetic methods below.

Isolation of ethyl-*p*-methoxycinnamate (1). The dried aromatic ginger (*Kaempferia galanga* L.) was chopped using a blender until smooth and became a powder. Totally 30 g of aromatic ginger was extracted by the soxhletation method in *n*-hexane solvent for 6 h. The mixture was filtered and evaporated until the volume was about 10 mL. The mixture was cooled at room temperature until white crystals were formed. The pureness of the crystal was tested in TLC, and the melting point was also determined. Pure crystals were weighed and characterized using FTIR spectrophotometers. A white crystal with a melting point of 46–48 °C (0.33% of yield). FTIR (KBr): ν (cm^{-1}) 3000–3100 (C-H sp^2), 2980.02 (C-H sp^3), 1707 (C=O ester), 1633.71 (C=C olefin), 1421.54 and 1367.53 (CH_3), 1253.73 (C-O phenolic), 1168.86 (C-O methoxy), 983.70 (1.2-disubstituted), and 829.39 (*para*-disubstituted aromatic).

***p*-Methoxycinnamate acid (2).** A white crystal with a melting point of 166–168 °C and 77.91% of yield. FTIR (KBr): ν (cm^{-1}) 3200 (O-H carboxylate), 3000–3100 (C-H sp^2), 2935.66 (C-H sp^3), 1683.86 (C=O carboxylate), 1624.06 (C=C olefin), 1595.13 and 1510 (C=C aromatic), 1255.56 (C-O phenolic), 1168.86 (C-O methoxy), and 941.26 (C=C olefin *trans* 1.2-disubstituted).

***p*-Methoxycinnamoil chloride (3).** A pale-yellow crystal. There was no spectroscopy data due to the rapidness of the compound changing to an acidic form (**1**).

***N*-phenethyl-*p*-methoxycinnamamide (4a).** A white crystal with a melting point of 110–112 °C and 42% of yield. FTIR (KBr): ν (cm^{-1}) 3269.34 (-NH), 3057.17 (C-H saturation), 2931.80 (C-H sp3), 1654.92 (C=O amide), 1620.00 (C=C olefin), 1450.47 (C-N), 1253.73 (C-O phenolic), and 829.39 (*para* disubstituted Ar). ^{1}H-NMR (500 MHz, chloroform-*d*) δ, ppm: 7.57 and 6.20 (2H, *d*, *J* = 15.55 Hz), 7.42 (2H, *d*, *J* = 8.75 Hz), 7.25 (5H, *m*, aromatic), 6.86 (2H, *d*, *J* = 8.75), 5.72 (1H, s, N-H amide), 3.81 (3H, *s*, methoxy), 3.64 (2H, *q*, *J* = 6.65 Hz), and 2.88 (2H, *t*, *J* = 6.95 Hz). ^{13}C-NMR (125 MHz, chloroform-*d*) δ, ppm: 166.36 (C-1), 160.96 (C-7), 140.75 (C-3), 139.07 (C-3'), 129.45 (C-5 and C-9), 128.78 (C-4' and C-8'), 128.63 (C-7' and C-5'), 127.62 (C-4),

126.63 (C-6'), 118.33 (C-2), 114.32 (C-6 and C-8), 55.45 (C-10), 40.90 (C-1'), and 35.83 (C-2').

***N*-morpholinyl-*p*-methoxycinnamamide (4b).** A pale-yellow crystal with a melting point of 96–98 °C and 16.04% of yield. FTIR (KBr): ν (cm^{-1}) 3061 (C-H sp^2), 2854–2922 (C-H saturation), 1647 (C=O amide conjugated), 1512 and 1600 (C=C aromatic), 1305 and 1433 (-CH^3 and -CH^2-), 1255 (-C-N amide), 1112 (C-O ether), 821 (*para*-substituted Ar), and 979 (C-H olefin trans), ^{1}H-NMR (500 MHz, chloroform-*d*) δ, ppm: 7.6574 (1H, *d*, *J* = 15.2 Hz), 7.4633 (2H, *d*, *J* = 8.7 Hz),), 6.8845 (2H, *d*, *J* = 8.3 Hz), 6.7039 (1H, *d*, *J* = 15.4 Hz, 3.8208 (3H, *s*), and 3.6857 (8H, *m*). ^{13}C-NMR (125 MHz, chloroform-*d*) δ, ppm: 165.98 (C-1), 143.05 (C-3), 129.49 (C-5), 127.95 (C-4), 114.34 (C-8), 114.06 (C-2), 66.99 (C-2'), 61.05 (C-7), 55.47 (C-10), 46.30 (C-1'), and 42.59 (C-3').

Bioactivity assay as an α-glucosidase inhibitor

The procedure of bioactivity test was conducted according to the procedure reported by Kim et al. [27]. About 0.2 mL of various concentrations of the tested samples 62.5, 125, 250, 500, and 1000 ppm were added with 0.5 mL *p*-nitrophenyl-α-D-glucopyranose 10 mM and 5 mL buffer phosphate (pH = 7). The mixture was incubated at 37 °C for 5 min, then added 0.2 mL α-glucosidase enzyme. Further incubation was done at 37 °C for 20 min. Each mixture was taken as much as 2 mL, then added 8 mL Na_2CO_3 0.1 M. All samples measured the absorbance using a spectrophotometer UV-Vis (λ_{max} 350–500 nm) in triplicates. Percent of inhibition was obtained by using Eq. (1).

$$\text{Percent of inhibition } (\%) = \frac{A_{control} - A_{sample}}{A_{control}} \times 100\% \qquad (1)$$

Homology modeling

Due to the absence of crystal structure of the α-glucosidase enzyme from rice in the protein data bank, homology modeling was carried out. The 3D structure of the α-glucosidase inhibitor was built by using the SWISS-MODEL workspace [28]. The FASTA format of α-glucosidase code B9F676 was submitted to run the homology model. The high similarity of the resulting model was evaluated through the Ramachandran plot [29].

Molecular docking

Molecular docking of compounds **4a** and **4b** through α-glucosidase was performed in the AutoDock4 program [30]. The crystal structure of the α-glucosidase enzyme was obtained from the result of the homology modeling stage. Each ligand (**4a** and **4b**) was optimized and prepared for docking in Chimera software [31]. Ligands were set in the active site of the enzyme, and the box grid size used was $50 \times 50 \times 50$ Å^3. The *xyz* coordinates of ligands were 2.532, 9.116, and 9.491, respectively, and the spacing was 0.375 Å. All ligands were arranged to produce ten conformations using the Lamarckian Genetic Algorithm [32]and visualized by the Discovery Studio Visualizer program [33].

Molecular dynamics simulation

The data of complex protein-ligand from the molecular docking was continued to molecular dynamics simulation using YASARA Dynamics software (YASARA Biosciences GmBH, Vienna, Austria) [34]. The simulation was carried out by using Amber14 force fields [35] in a periodic boundary condition, and each complex was set to have a temperature and pH physiologic of 310 K and 7.4, respectively [36]. Solvation of the complex was set in TIP3P solvent [37], and counter ions (Na^+, Cl^-) were added to normalize the system. The time step used in this simulation is 0.25 fs, and all the trajectory data was collected every 25 ps. Finally, all the complexes were running in 10 ns, and trajectory data was employed to analyze the root mean square deviation (RMSD) of carbon alpha, RMSD total of the system, RMSD ligands, root mean square fluctuation (RMSF), the radius of gyration, and Molecular Mechanics Poison-Boltzmann Surface Area (MM-PBSA) energy.

■ RESULTS AND DISCUSSION

Conversion and Characterization

In this study, the substrate, ethyl-*p*-methoxycinnamate (EPMC), was obtained from aromatic ginger (*Kaempferia galanga* L.) due to the high content of this compound had been reported [9]. In the isolation method, the percent of the yield was about 0.33%. The others research reported a variation of yield

such as 0.98% [1], 0.57% [11], and 0.026% [38]. The difference in yield can be caused by the difference in isolation methods such as extraction method, the solvent used, and extraction time.

FTIR spectra indicated that the crystal belongs to EPMC (**1**) due to the absorption at 1707 cm^{-1} of the carbonyl ester strengthened by the band at 1186.86 cm^{-1} of C-O from the ethyl group. Moreover, the absorption band appearing between 3000–3100 cm^{-1} indicated the presence of an aromatic ring, which was supported by the band at 1512.19 and 1604 cm^{-1}. In addition, the absorption at 829.39 cm^{-1} showed that this aromatic group had *para* di-substituents which also gave overtone at 1890.24 cm^{-1}. The vibration at 1633.71 cm^{-1} indicated the presence of C=C olefin, which was supported by the band at 983.70 cm^{-1} of *trans* 1,2-disubstituted olefin. These FTIR spectra followed the previous study about the isolation of EPMC [11]. Due to the hygroscopic property of isolated EPMC, no further spectroscopic data was performed, and it was directly converted to *p*-methoxycinnamate acid (**2**) by hydrolysis in alkaline conditions. A successful hydrolysis reaction was seen in the FTIR spectra of the crystal due to the presence of stretching O-H absorption between 2750–3200 cm^{-1}. Moreover, absorption of C=O obtained in 1683.86 cm^{-1} indicated that the carbonyl group belongs to a carboxylic acid moiety.

The melting point value of isolated EMPC had a range value of 46–48 °C, and this value was quite similar to the result of Umar et al. [38], who had isolated and obtained the melting point of EMPC was about 49 °C. The difference in melting point value may be due to the different conditions of the tested location, such as pressure or temperature. The same thing was also found in the melting point of *p*-methoxycinnamate acid (**2**), the resulting melting point was about 166–168 °C, and the melting point of **2** based on the data in the chemical safety data sheet is about 170–173 °C.

Chlorination of **2** was done in four hours (based on TLC control) by the addition of thionyl chloride. This chlorination step was conducted to increase the reactivity of the carbonyl group before amidation. The structure of this reaction product was expected to be **3**. However, in this stage, no spectroscopy data resulted because the crystal was simply returned to its acidic form by moisture conditions. Therefore, the amidation stage was directly carried out after chlorination (*in situ* process). In this step, two amine compounds were used, namely phenethylamine and morpholine, to produce *N*-phenethyl-*p*-methoxycinnamamide (**4a)** and *N*-morpholinyl-*p*-methoxycinnamamide (**4b**), respectively. Pyridine and triethylamine were used in the reaction mixture to bind HCl which was produced as a by-product in both amidation reactions. The synthesis pathways of **4a** and **4b** from EPMC are shown in Scheme 1.

The structure of both amidation products was confirmed by FTIR, ^{1}H-NMR, and ^{13}C-NMR spectra. In FTIR spectra of **4a**, there was a short single peak at 3269.34 cm^{-1} that belongs to the N-H group, while spectra of **4b** showed no absorption band between 3200–3400 cm^{-1} because it is a tertiary amide. Vibration at 1654.92 cm^{-1} (**4a**) and 1647.21 cm^{-1} (**4b**) corresponded to C=O conjugated from the amide group that was supported by vibration at 1450.47 cm^{-1} (**4a**) and 1433.11 cm^{-1} (**4b**) of C-N stretching bands. In addition, the presence of the phenethyl group in **4a** was also confirmed by the absorption band at 746.45 and 700.16 cm^{-1}, indicating the presence of an additional mono-substituted aromatic ring.

^{13}C-NMR spectra of compound **4a** showed 14 signals representing 18 carbons and 11 signals exhibiting 14 carbon atoms for compound **4b**. In compound **4a**, four pairs of aromatic carbon atoms, namely C-5 and C-9, C-6 and C-8, C-7' and C-5', as well as C-4' and C-8', had identical chemical environments, thus appearing as only eight signals together with the signals of C-4, C-7, C-3' and C-6' between 114–140 ppm. Similarly, the aromatic carbon atoms of **4b** were shown by four signals at δ 161.05,129.49, 114.34, and 27. 95 ppm from C-7, C-5 and C-9, C-6, and C-8, as well as C-4, respectively. C-1' and C-2' of compound **4a** appeared as the two most shielding signals (δ 40.90 and 35.83 ppm) due to their position between N amide and the aromatic ring.

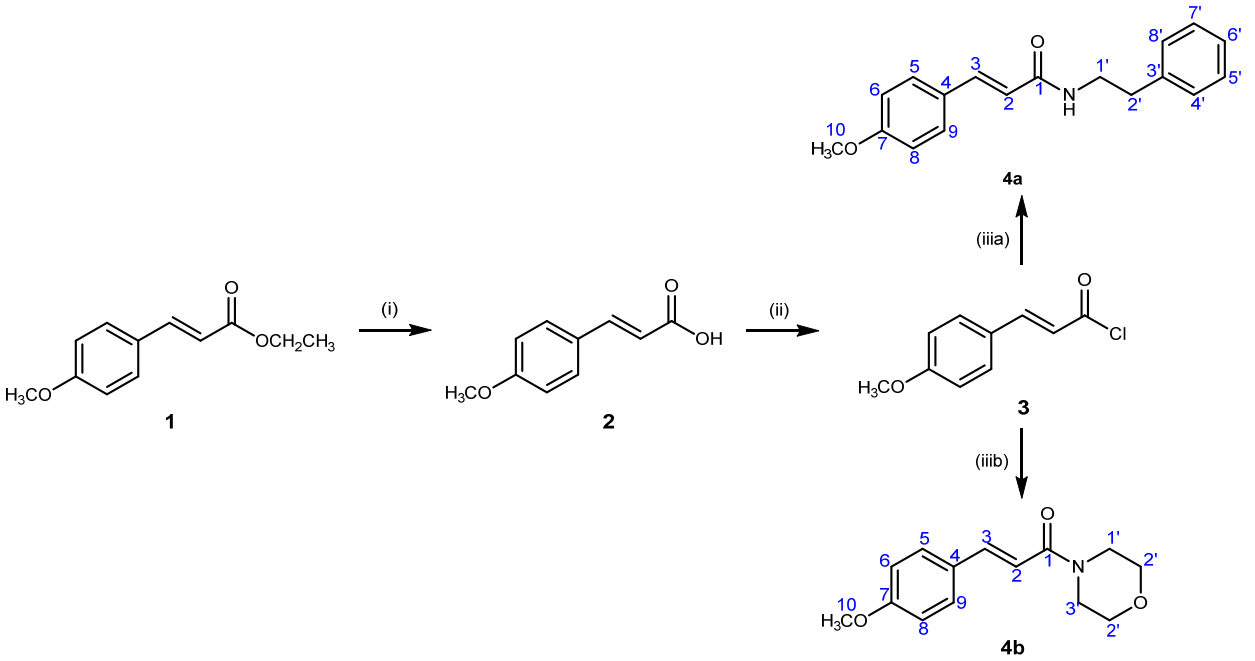

Scheme 1. Synthesis pathways of **4a** and **4b**: (i) hydrolysis (NaOH/EtOH, reflux 60 °C, 3 h); (ii) chlorination ($SOCl_2$/EtOH, reflux 78 °C, 4 h); (iiia) amidation-a (phenethylamine, pyridine, and Ph_3N in chloroform, r.t., 4 h); (iiib) amidation-b (morpholine, pyridine, and Et_3N in chloroform, r.t., 4 h)

For compound **4b**, the most shielding signals were from C-1' and C-3' of morpholine moiety. Both signals appeared in different chemical shifts because the morpholine ring had an envelope conformation, which cannot be inverted at room temperature [39]. C-1' was closer to the oxygen of the carbonyl group than C-3', and C-1' appeared at a more deshielding chemical shift than C-3'. A signal at δ 66.99 ppm confirmed the two C-2' atoms of morpholine moiety, which are next to the oxygen atom. These results were in line with previous studies, which confirmed the presence of morpholine moiety by these three signals in their ^{13}C-NMR spectra [40-41]. Moreover, the most deshielding atoms of both compounds were C-1 (carbonyl carbon) and C-7 (aromatic carbon next to oxygen). The signals at δ 55.45 and 55.46 ppm represented methoxy carbon atom (C-10) of both **4a** and **4b**, respectively. In addition, the ^{1}H-NMR spectra of these compounds also supported the structural elucidation of **4a** and **4b**, which show nine signal groups from 19 proton units and six signal groups from 17 proton units, respectively. All proton signals followed the chemical structure of **4a** and **4b** as *N*-phenethyl-*p*-methoxycinnamamide and *N*-morpholinyl-*p*-methoxycinnamamide, respectively.

Bioactivity Study

The newly cinnamamide derivatives were tested as α-glucosidase inhibitors due to a large number of studies reporting that cinnamic acid derivatives had the potential as antidiabetic through inhibition of the α-glucosidase enzyme. This enzyme was isolated from rice, and acarbose was used as a positive control in this study. The result of the inhibitory test was found that compound **4b** has a better inhibition (IC_{50}) value of 1.83×10^{-2} M than **4a** was about 2.65×10^{-2} M. Both compounds still had a lower inhibition property if compared to acarbose (1.43×10^{-3} M). Differentiation of activity from both compounds can be caused by the differences in molecular volumes of each compound. Compound **4b** had a more compact structure than **4a**, which had a phenethyl moiety. Structure comparison between **4a** and compound **1a** from another study (Fig. 1) showed that the methoxy group could influence bioactivity. In **1a**, which had a hydroxyl group, could

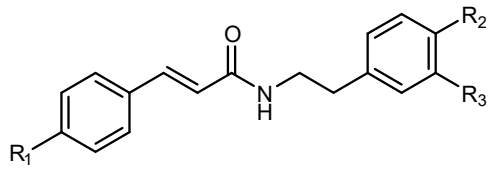

	R_1	R_2	R_3	IC_{50}	Reference
4a	OCH_3	H	H	2.65×10^{-2} M	Present study
1a	OH	H	H	3.10×10^{-7} M	[20]
1d	H	OH	H	2.15×10^{-4} M	[20]

Fig 1. Structure and bioactivity of cinnamamide derivatives as an α-glucosidase inhibitor

make inhibition activity stronger than if the hydroxyl group was changed to methoxy or hydrogen (**1d**) [20]. This result showed that there is a relationship between structure and compound activity.

Homology Modeling

The crystal structure of α-glucosidase from rice has never been isolated before, and it makes some studies did homology modeling to create the sequence of the α-glucosidase enzyme [23,29]. Another study has been attempted using different programs such as SWISS-MODEL and PBD ID 2G3M but only gave a similarity identity of about 31.35% [42], and our study resulting a better similarity index. Fig. 2 presented the result of homology modeling, showing that murine endoplasmic reticulum α-glucosidase II (PDB ID: 5IED) has a high sequence similarity index of 79%. The resulting model was validated using the Ramachandran plot, which describes the quality model through psi and phi angle. It was implied that the resulting model has a good quality due to almost residue being in the favored region (92.01%), 4.76% residue in the allowed region, 1.32% residue was rotamers outliers, and only 1.91% residue grouping as Ramachandran outliers. This model then continued to use in the molecular docking stage.

Molecular Docking

Molecular docking analysis was carried out to find the interactions between two cinnamamide derivatives (**4a** and **4b**) against the α-glucosidase enzyme. Fig. 3(a) displayed the two-dimension interaction between **4a** and α-glucosidase enzyme. There were many interactions contributed, such as van der Waals and C-H bond that usually appeared in the docking results. Despite the absence of a hydrogen bond, there were many π stacking interactions against protein residue, such as π-anion interactions with Asp397 and π-sulfur with Met511. The interaction between ligand **4b** with α-glucosidase enzyme displayed in Fig. 3(b) showed that there was an additional interaction that was not found in **4a**, which was a hydrogen bond with His644 and Phe263.

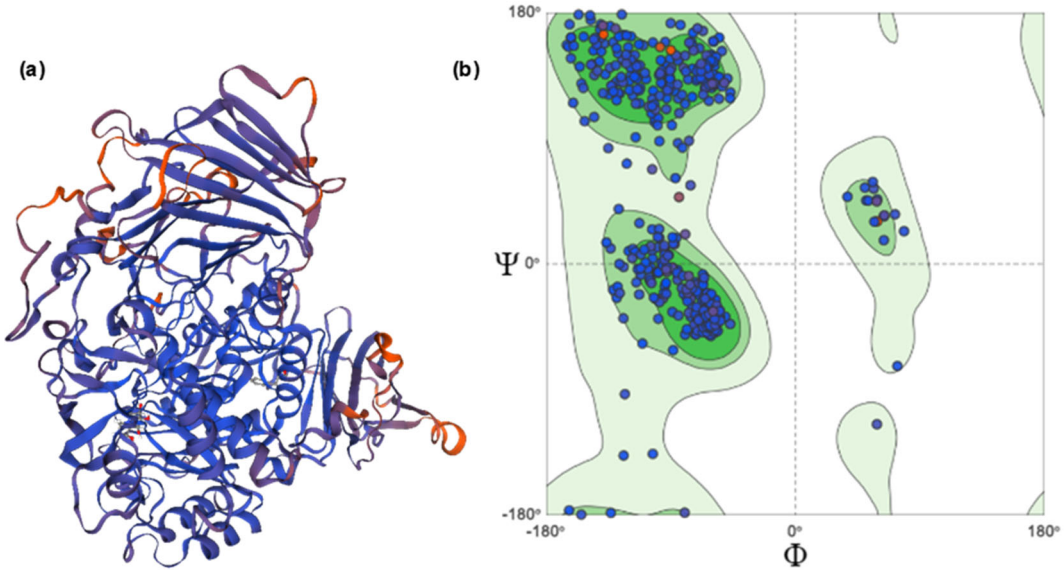

Fig 2. The crystal structure resulted from homology modeling (a) and Ramachandran plot of the resulting homology model (b)

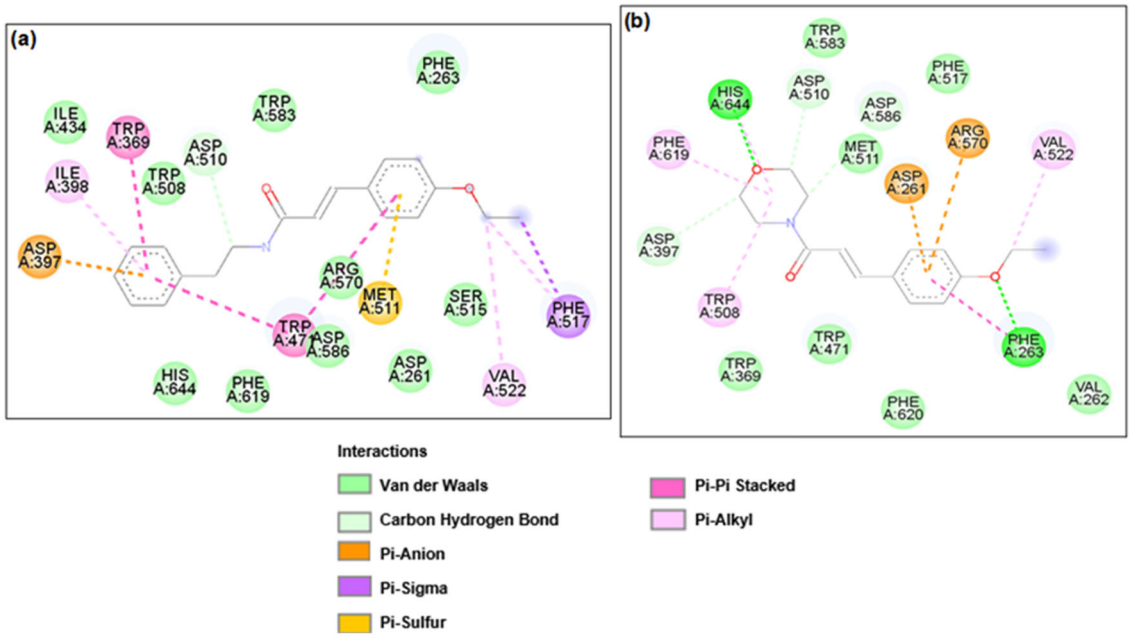

Fig 3. 2D-Interaction of (a) **4a** and (b) **4b** against α-glucosidase enzyme

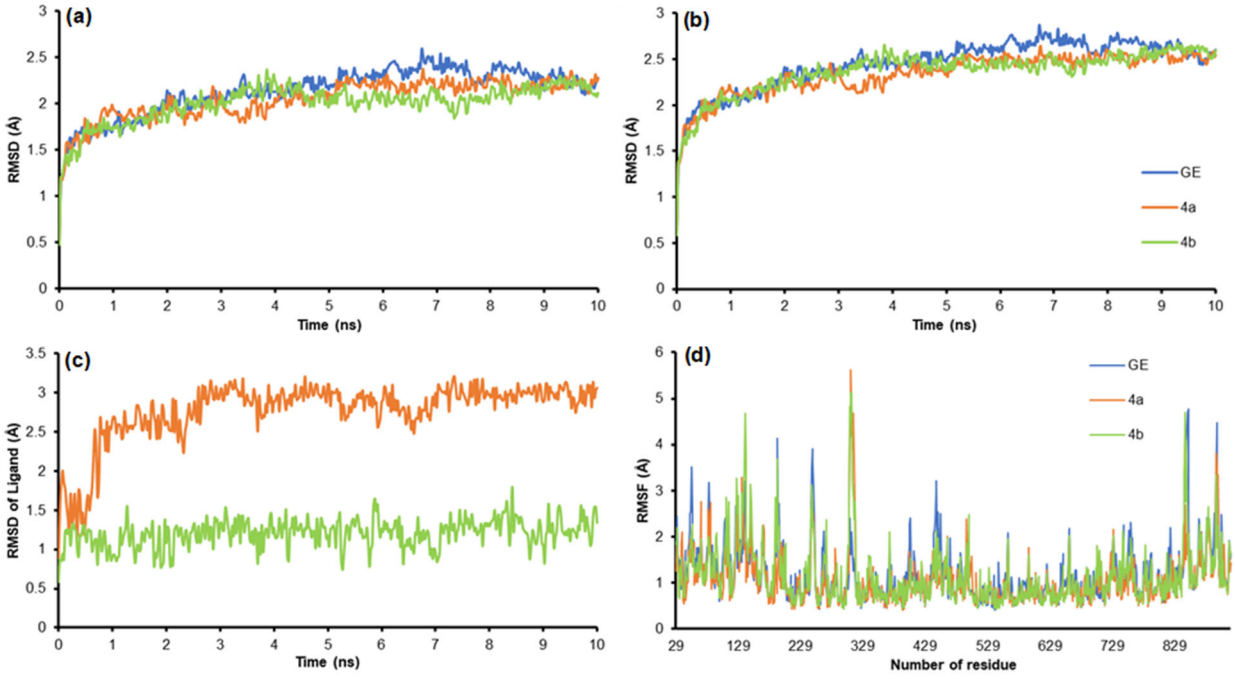

Fig 4. Result of molecular dynamics simulation (a) RMSD of Cα graph (b) RMSD total graph (c) RMSD of ligand and (d) root mean square fluctuation (RMSF) graph

This additional interaction made the **4b** compound bind strongly with the enzyme. It was also in line with the result of the binding energy calculation that compounds **4a** and **4b** had binding energy of -29.7064 and -30.1666 kJ mol^{-1}, respectively.

Molecular Dynamics Simulation

The protein and ligand complex resulting in docking analysis was subjected to molecular dynamics simulation to evaluate the interaction stability. Fig. 4(a) and 4(b) presented the root mean square deviation (RMSD) graph

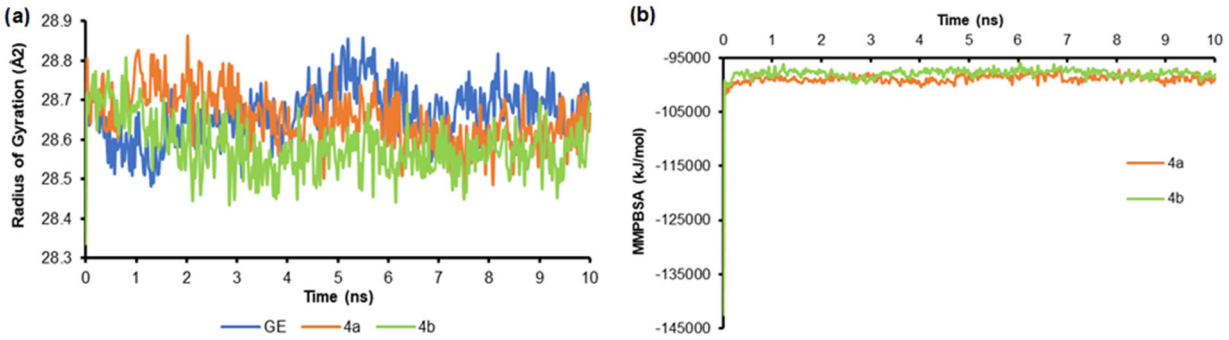

Fig 5. (a) Radius of gyration plot of glucosidase enzyme (GE) compared with the complex of GE and ligand (b) MM-PBSA plot of each ligand

of carbon alpha and RMSD total of each complex compared with the α-glucosidase enzyme. All complexes showed the RMSD value around 2 until 2.5 Å, indicating that the addition of ligands did not make any significant change in the structure of the enzyme. It was also supported by the result of root mean square fluctuation (RMSF) data (Fig. 4(d)), which showed that the addition of ligand in the structure of the enzyme did not change the number of residues significantly. Simulation in 10 ns also exhibited that ligand **4b** had a more stable structure than **4a** because of the lower RMSD value (Fig. 4(c)). The higher deviation of structure **4a** can be caused by the presence of the methylene group.

Evaluation of the complex equilibrium was done by checking the radius of gyration from each complex. Fig. 5(a) presents the analysis results that the minimum value of the graph shows the protein condition in a folded term. On the other hand, the maximum value presents the protein conformation when unfolded condition [43]. A comparison between a single protein and the protein complexing with ligands showed that the addition of ligands did not change the whole conformation of the protein due to the lower fluctuation. The complex energy was also evaluated using Molecular Mechanics Poison-Boltzmann Surface Area (MM-PBSA) method [44], which is shown in Fig. 5(b). After 10 ns simulation time, the energy of complex **4a** and **4b** was quite similar and stable during simulation time. The average binding energy value of ligands **4a** and **4b** was -98980.8 and -97696.7 kJ mol^{-1}. This binding energy was in line with the RMSD plot.

■ CONCLUSION

Ethyl-*p*-methoxycinnamate isolated from aromatic ginger (*Kaempferia galanga* L.) was successfully converted into two amide compounds, namely *N*-phenethyl-*p*-methoxycinnamamide and *N*-morpholinyl-*p*-methoxycinnamamide. Both compounds had a melting point of 110–120 and 96–98 °C, respectively. Spectroscopy data from FTIR, ^{1}H-, and ^{13}C-NMR showed the presence of peaks to prove the successful synthesis stage. *In vitro* bioactivity test was resulting that compound **4b** had a better IC_{50} value of about 1.83×10^{-2} M. Binding energy result of compounds **4a** and **4b** in molecular dynamics simulation had a near value of about -98980.8 and -97696.7 kJ mol^{-1}, respectively. Stability analysis of each complex in molecular dynamics simulation showed that the addition of ligand did not significantly change the structure of the enzyme. Furthermore, *in vitro* result was supported by *in silico* test using molecular docking and molecular dynamics simulation.

■ ACKNOWLEDGMENTS

The authors thank Institute for Research and Community Service, Hasanuddin University, for the research grant (No. 1476/UN4.22/PT.01.03/2022) in the scheme of Basic Research in 2022.

■ AUTHOR CONTRIBUTIONS

Herlina Rasyid conducted research design, writing, homology modeling, and molecular docking. Firdaus, Nunuk Hariani Soekamto, Syadza Firdausiah, and

Seniwati conducted the synthesis process and bioactivity test, Reynaldi and Andi Eka Sri Rahayu conducted the conversion stage, Riska Mardiyanti conducted writing and formatting article, and Wahyu Dita Saputri conducted molecular dynamics simulation, writing, and revising the manuscript. All authors agreed to the final version of this manuscript.

■ REFERENCES

[1] Hakim, A., Andayani, Y., and Rahayuan D.R., 2018, Isolation of ethyl-*p*-methoxy cinnamate from *Kaemferia galanga* L, *J. Phys.: Conf. Ser.*, 1095 (1), 012039.

[2] Singh, S., Sahoo, S., Sahoo, B.C., Kar, B., Dash, M., Nayak, S., and Kar, B., 2022, Derivatives of cinnamic acid esters and terpenic diversity in volatiles of thirty-six sand ginger (*Kaempferia galanga* L.) accessions of Eastern India revealing quality chemovars, *Molecules*, 27 (3), 1116.

[3] Wisetsai, A., Schevenels, F.T., Kanokmedhakul, S., Kanokmedhakul, K., Boonmak, J., Youngme, S., Suebrasri, T., and Lekphrom, R., 2021, Isopimarane-type diterpenoids from the rhizomes of *Kaempferia galanga* L. and their biological activities, *Nat. Prod. Res.*, 1–10.

[4] Elshamy, A.I., Mohamed, T.A., Swapana, N., Ahmed, R.F., Yoneyama, T., Paré, P.W., Noji, M., Hegazy, M.E.F., and Umeyama, A., 2021, Two new diterpenoids from kencur (*Kaempferia galanga*): Structure elucidation and chemosystematic significance, *Phytochem. Lett.*, 44, 185–189.

[5] Raina, A.P., and Abraham, Z., 2016, Chemical profiling of essential oil of *Kaempferia galanga* L. germplasm from India, *J. Essent. Oil Res.*, 28 (1), 29–34.

[6] Firdaus, F., Soekamto, N.H., Seniwati, S., Firdausiah, S., Rasyid, H., Bahja, B., and Islam, M.F., 2021, Phenethyl *p*-coumarate and *N*-Phenethyl-*p*-coumaramide: Synthesis, characterization. docking studies, and anticancer activity through P388 cell, *Sains Malays.*, 51 (4), 1085–1097.

[7] Firdaus, F., Seniwati, S., Alamsyah, N., and Paramita, S., 2019, Synthesis and activity of *N*-(*o*-tolyl)caffeamide and *N*-(*o*-tolyl)-*p*-coumaramide against P388 leukemia murine cells, *J. Phys.: Conf. Ser.*, 1341, 032005.

[8] Zenta, F., Soekamto, N.H., Dali, S., Firdausiah, S., Rasyid, H., Bahriah, B., Agustan, A., and Tahir, D., 2022, Development *trans-N*-benzyl hydroxyl cinnamamide based compounds from cinnamic acids and characteristics anticancer potency, *J. Iran. Chem. Soc.*, 19, 2845–2853.

[9] Umar, M.I., Asmawi, M.Z., Sadikun, A., Atangwho, I.J., Yam, M.F., Altaf, R., and Ahmed, A., 2012, Bioactivity-guided isolation of ethyl-*p*-methoxycinnamate, an anti-inflammatory constituent, from *Kaempferia galanga* L. extracts, *Molecules*, 17 (7), 8720–8734.

[10] Komala, I., Supandi, S., Nurhasni, N., Betha, O.S., Putri, E., Mufidah, S., Awaludin, M.F., Fahmi, M., Reza, M., and Indriyani, N.P., 2018, Structure-activity relationship study on the ethyl *p*-methoxycinnamate as an anti-inflammatory agent, *Indones. J. Chem.*, 18 (1), 60–65.

[11] Lakshmanan, D., Werngren, J., Jose, L., Suja, K.P., Nair, M.S., Varma, R.L., Mundayoor, S., Hoffner, S., and Kumar, R.A., 2011, Ethyl *p*-methoxycinnamate isolated from a traditional anti-tuberculosis medicinal herb inhibits drug resistant strains of *Mycobacterium tuberculosis* in vitro, *Fitoterapia*, 82 (5), 757–761.

[12] Ichwan, S.J.A., Husin, A., Suriyah, W.H., Lestari, W., Omar, M.N., and Kasmuri, A.R., 2019, Anti-neoplastic potential of ethyl-*p*-methoxycinnamate of *Kaempferia galanga* on oral cancer cell lines, *Mater. Today: Proc.*, 16, 2115–2121.

[13] Guzman, J.D., 2014, Natural cinnamic acids, synthetic derivatives and hybrids with antimicrobial activity, *Molecules*, 19 (12), 19292–19349.

[14] Chowdhury, M.Z., Al Mahmud, Z., Ali, M.S., and Bachar, S.C., 2014, Phytochemical and pharmacological investigations of rhizome extracts of *Kaempferia galanga*, *Int. J. Pharmacogn.*, 1 (3), 185–192.

[15] Sudatri, N.W., Wirasiti, N., Gde Bidura, I.G.N., and Suartini, N.M., 2019, Anti-diabetic and anti-

cholesterol activity of Kaempferia galanga L. herbal medicine rhizome in albino rats, *Int. J. Fauna Biol. Stud.*, 6 (5), 13–17.

[16] Adisakwattana, S., Roengsamran, S., Hsu, W.H., and Yibchok-Anun, S., 2005, Mechanisms of antihyperglycemic effect of *p*-methoxycinnamic acid in normal and streptozotocin-induced diabetic rats, *Life Sci.*, 78 (4), 406–412.

[17] Adisakwattana, S., Sompong, W., Meeprom, A., Ngamukote, S., and Yibchok-anun, S., 2012, Cinnamic acid and its derivatives inhibit fructose-mediated protein glycation, *Int. J. Mol. Sci.*, 13 (2), 1778–1789.

[18] Ernawati, T., Radji, M., Hanafi, M., Mun'im, A., and Yanuar, A., 2017, Cinnamic acid derivatives as α-glucosidase inhibitor agents, *Indones. J. Chem.*, 17 (1), 151–160.

[19] Ernawati, T., Mun'im, A., Hanafi, M., and Yanuar, A., 2020, Synthesis of cinnamamide derivatives and their α-glucosidase inhibitory activities, *Sains Malays.*, 49 (2), 315–322.

[20] Song, Y.H., Kim, D.W., Curtis-Long, M.J., Park, C., Son, M., Kim, J.Y., Yuk, H.J., Lee, K.W., and Park, K.H., 2016, Cinnamic acid amides from *Tribulus terrestris* displaying uncompetitive α-glucosidase inhibition, *Eur. J. Med. Chem.*, 114, 201–208.

[21] Guerreiro, L.R., Carreiro, E.P., Fernandes, L., Cardote, T.A.F., Moreira, R., Caldeira, A.T., Guedes, R.C., and Burke, A.J., 2013, Five-membered iminocyclitol α-glucosidase inhibitors: Synthetic, biological screening and in silico studies, *Bioorg. Med. Chem.*, 21 (7), 1911–1917.

[22] Khan, K.M., Rahim, F., Wadood, A., Kosar, N., Taha, M., Lalani, S., Khan, A., Fakhri, M.I., Junaid, M., Rehman, W., Khan, M., Perveen, S., Sajid, M., and Choudhary, M.I., 2014, Synthesis and molecular docking studies of potent α-glucosidase inhibitors based on biscoumarin skeleton, *Eur. J. Med. Chem.*, 81, 245–252.

[23] Rahim, F., Zaman, K., Taha, M., Ullah, H., Ghufran, M., Wadood, A., Rehman, W., Uddin, N., Shah, S.A.A., Sajid, M., Nawaz, F., and Khan, K.M., 2020, Synthesis, *in vitro* alpha-glucosidase inhibitory potential of benzimidazole bearing *bis*-Schiff bases and their molecular docking study, *Bioorg. Chem.*, 94, 103394.

[24] Rahman, N., Muhammad, I., Nayab, G.E., Khan, H., Aschner, M., Filosa, R., and Daglia, M., 2019, Molecular docking of isolated alkaloids for possible α-glucosidase inhibition, *Biomolecules*, 9 (10), 544.

[25] Mollica, A., Zengin, G., Durdagi, S., Ekhteiari Salmas, R., Macedonio, G., Stefanucci, A., Dimmito, M.P., and Novellino, E., 2019, Combinatorial peptide library screening for discovery of diverse α-glucosidase inhibitors using molecular dynamics simulations and binary QSAR models, *J. Biomol. Struct. Dyn.*, 37 (3), 726–740.

[26] Azimi, F., Ghasemi, J.B., Azizian, H., Najafi, M., Faramarzi, M.A., Saghaei, L., Sadeghi-aliabadi, H., Larijani, B., Hassanzadeh, F., and Mahdavi, M., 2021, Design and synthesis of novel pyrazole-phenyl semicarbazone derivatives as potential α-glucosidase inhibitor: Kinetics and molecular dynamics simulation study, *Int. J. Biol. Macromol.*, 166, 1082–1095.

[27] Kim, Y.M., Wang, M.H., and Rhee, H.I., 2004, A novel α-glucosidase inhibitor from pine bark, *Carbohydr. Res.*, 339 (3), 715–717.

[28] Waterhouse, A., Bertoni, M., Bienert, S., Studer, G., Tauriello, G., Gumienny, R., Heer, F.T., de Beer, T.A.P., Rempfer, C., Bordoli, L., Lepore, R., and Schwede, T., 2018, SWISS-MODEL: Homology modelling of protein structures and complexes, *Nucleic Acids Res.*, 46 (W1), W296–W303.

[29] Wang, G., Peng, Z., Wang, J., Li, X., and Li, J., 2017, Synthesis, *in vitro* evaluation and molecular docking studies of novel triazine-triazole derivatives as potential α-glucosidase inhibitors, *Eur. J. Med. Chem.*, 125, 423–429.

[30] Morris, G.M., Huey, R., Lindstrom, W., Sanner, M.F., Belew, R.K., Goodsell, D.S., and Olson, A.J., 2009, AutoDock4 and AutoDockTools4: Automated docking with selective receptor flexibility, *J. Comput. Chem.*, 30 (16), 2785–2791.

[31] Pettersen, E.F., Goddard, T.D., Huang, C.C., Couch, G.S., Greenblatt, D.M., Meng, E., and

Ferrin, T.E., 2004, UCSF Chimera – A visualization system for exploratory research and analysis, *J. Comput. Chem.*, 25 (13), 1605–1612.

[32] Morris, G.M., Goodsell, D.S., Halliday, R.S., Huey, R., Hart, W.E., Belew, R.K., and Olson, A.J., 1998, Automated docking using a Lamarckian genetic algorithm and an empirical binding free energy function, *J. Comput. Chem.*, 19 (14), 1639–1662.

[33] BIOVIA, 2019, *Discovery Studio Visualizer*, Dassault Systèmes, San Diego.

[34] Land, H., and Humble, M.S., 2018, YASARA: A tool to obtain structural guidance in biocatalytic investigations, *Methods Mol. Biol.*, 1685, 43–67.

[35] Wang, J., Wolf, R.M., Caldwell, J.W., Kollman, P.A., and Case, D.A., 2004, Development and testing of a general AMBER force field, *J. Comput. Chem.*, 25 (9), 1157–1174.

[36] Dash, R., Ali, M.C., Dash, N., Azad, M.A.K., Zahid Hosen, S.M., Hannan, M.A., and Moon, I.S., 2019, Structural and dynamic characterizations highlight the deleterious role of SULT1A1 R213H polymorphism in substrate binding, *Int. J. Mol. Sci.*, 20 (24), 6256.

[37] Mark, P., and Nilsson, L., 2001, Structure and dynamics of the TIP3P, SPC, and SPC/E water models at 298 K, *J. Phys. Chem. A*, 105 (43), 9954–9960.

[38] Umar, M.I., Asmawi, M.Z., Sadikun, A., Majid, A.M.S.A., Al-Suede, F.S.R., Hassan, L.E.A., Altaf, R., and Ahamed, M.B.K., 2014, Ethyl-*p*-methoxycinnamate isolated from *Kaempferia galanga* inhibits inflammation by suppressing interleukin-1, tumor necrosis factor-α, and angiogenesis by blocking endothelial functions, *Clinics*, 69 (2), 134–144.

[39] El-Gogary, T.M., and Soliman, M.S., 2001, Ab-Initio molecular geometry and normal coordinate analysis of pyrrolidine molecule, *Spectrochim. Acta, Part A*, 57 (13), 2647–2657.

[40] Firdaus, F., Soekamto, N.H., Firdausiah, S., Rasyid, H., Asmi, N., and Waleulu, M., 2021, Novel hydroxycinnamamide from morpholine and pyrrolidine: Synthesis, characterization, docking study, and anticancer activity against P388 leukemia murine cells, *J. Appl. Pharm. Sci.*, 11 (01), 40–48.

[41] Firdaus, F., Husain, D.R., Naid, T., Seniwati, S., Soekamto, N.H., Sumarna, S., and Islam, M.F., 2017, Synthesis of piperidine and morpholine amides of ferulic acid and their bioactivity against P-388 leukemia cells, *Int. J. ChemTech. Res.*, 10 (1), 27–33.

[42] Ernawati, T., Mun'im, A., Hanafi, M., and Yanuar, A., 2017, Design of cinnamic acid derivatives and molecular docking toward human-neutral a-glucosidase by using homology modeling, *Orient. J. Chem.*, 33 (5), 2249–2256.

[43] Yamamoto, E., Akimoto, T., Mitsutake, A., and Metzler, R., 2021, Universal relation between instantaneous diffusivity and radius of gyration of proteins in aqueous solution, *Phys. Rev. Lett.*, 126 (12), 128101.

[44] Miller, B.R., Mcgee, T.D., Swails, J.M., Homeyer, N., Gohlke, H., and Roitberg, A.E., 2012, MMPBSA.py: An efficient program for end-state free energy calculations, *J. Chem. Theory Comput.*, 8 (9), 3314–3321.